

# Predicting Patagonian Landslides: Roles of Forest Cover and Wind Speed

Eric Parra<sup>1</sup>, Christian Mohr<sup>1</sup>, and Oliver Korup<sup>1</sup>

<sup>1</sup>University of Potsdam

November 23, 2022

## Abstract

Dense tree stands and high wind speeds characterize the dense temperate rainforests of southern Chilean Patagonia, where landslides frequently strip hillslopes of soils, rock, and biomass. Assuming that wind loads on trees promote slope instability, we explore the role of forest cover and wind speed in predicting mapped landslides with a robust Bayesian logistic regression. We find that more crown openness and higher wind speeds credibly predict higher probabilities of detecting landslides moderately well regardless of topographic location, though much better in low-order channels and on midslope locations than on open slopes. Wind speed has less predictive power in areas that were smothered by tephra fall from recent volcanic eruptions, while the influence of forest cover remains.

1     **Predicting Patagonian Landslides: Roles of Forest Cover and Wind Speed**

2                     **Eric Parra<sup>1,2</sup>, Christian H. Mohr<sup>1</sup>, Oliver Korup<sup>1,2</sup>**

3     <sup>1</sup>Institute of Environmental Science and Geography, University of Potsdam, Germany

4     <sup>2</sup>Institute of Geosciences, University of Potsdam, Germany

5     Corresponding author: Eric Parra ([parrahormaza@uni-potsdam.de](mailto:parrahormaza@uni-potsdam.de))

6     **Key Points:**

- 7             • Wind speed and crown openness of forests can aid landslide prediction in temperate
- 8             rainforests of southern Chile;
- 9             • Volcanic disturbance appears to smooth out the role of wind speed;
- 10            • Distinguishing between landform types in a hierarchical model context improves the
- 11            average performance of the landslide classification.

12

13 **Abstract**

14 Dense tree stands and high wind speeds characterize the dense temperate rainforests of southern  
15 Chilean Patagonia, where landslides frequently strip hillslopes of soils, rock, and biomass.  
16 Assuming that wind loads on trees promote slope instability, we explore the role of forest cover  
17 and wind speed in predicting mapped landslides with a robust Bayesian logistic regression. We  
18 find that more crown openness and higher wind speeds credibly predict higher probabilities of  
19 detecting landslides moderately well regardless of topographic location, though much better in  
20 low-order channels and on midslope locations than on open slopes. Wind speed has less  
21 predictive power in areas that were smothered by tephra fall from recent volcanic eruptions,  
22 while the influence of forest cover remains.

23

24 **Plain Language Summary**

25 Chilean Patagonia is home to not only some of Earth's largest swaths of temperate rainforests,  
26 but also to strong winds. Landslides commonly occur on steep hillslopes and remove, transport  
27 and deposit soil, rock and vegetation. To predict which areas are more likely fail compared to  
28 others, landslide models are needed. We developed a data-driven model that predicts from forest  
29 cover and wind speed the probability of detecting landslide terrain. Our findings indicate that  
30 both forest cover and wind speed play important, yet previously underappreciated, roles in  
31 predicting landslides in dense temperate rainforest. The model performance differs if  
32 distinguishing between landform types and previous volcanic disturbance, which may override  
33 the comparable modest control of wind on landsliding. Our study is the first of its kind in one of  
34 the windiest spots on Earth, and encourages a more discerning approach to landslide prediction.

35 **1 Introduction**

36 Many of Earth's steepest, wettest, and rapidly denuding landscapes are covered by dense  
37 temperate rainforests. The forests of southeast Alaska, southwest New Zealand, or Chilean  
38 Patagonia are amongst the most dense and biomass-rich biomes worldwide (DellaSala, 2011).  
39 These forests store large amounts of organic carbon (Luyssaert et al., 2008; Mohr et al., 2017)  
40 but also experience frequent disturbances (Johnstone et al., 2016) such as earthquakes,  
41 landslides, avalanches, windstorms, or volcanic eruptions (Buma et al., 2019; Korup et al., 2019;  
42 Sommerfeld et al., 2018; Veblen & Alaback, 1996) and thus high rates of erosion and biomass  
43 turnover (Hilton et al., 2008; Hilton et al., 2011). Landslides in particular have both a destructive  
44 and vital role in these forest ecosystems by regulating biomass erosion and deposition, nutrient  
45 cycling, and stand succession (Pawlik, 2013). Forest disturbances, in turn, alter landslide  
46 susceptibility (Buma & Johnson, 2015), and reported landslide densities in forest areas can be  
47 50-90% lower than in open land, depending on forest type and health (Rickli & Graf, 2009).  
48 Studies of landsliding after deforestation revealed that the susceptibility to shallow landslides can  
49 increase because of limited root reinforcement (Sidle, 1991; Schwarz et al., 2010) and altered  
50 hydraulic conductivity (Mirus et al., 2017). But also biomass surcharge (O' Loughlin & Ziemer,  
51 1982) or trees transferring dynamic wind forces to the soil can trigger slope instability (Buma &  
52 Johnson, 2015).

53 Among these possible controls on slope stability in forested mountains, forest cover and wind  
54 speed have been the least considered in landslide prediction; most research instead addressed the  
55 less dynamic factors of geology and topography (Reichenbach et al., 2018).

56 Despite numerous studies on forest disturbances (Baumann et al., 2014) enquiries into the role of  
57 wind on landslide initiation have been anecdotal with unclear indications of cause and effect

58 (Buma & Johnson, 2015; Schwab, 1983). We suspect that forest cover and wind speed have  
59 opposite effects on slope stability. Despite anchoring soils, trees transfer dynamic wind forces as  
60 turning moments (torque) to the soil mantle via the tree bole, causing tree fall or even triggering  
61 shallow slope failure (Buma & Johnson, 2015). The torque depends mostly on wind speed  
62 (squared) and to lesser degree on tree physiology such as height or diameter (Hale et al., 2015).  
63 Storm-induced tree throw also displaces soil and opens up pits for enhanced water infiltration  
64 and pore-water pressure in soils (Valtera & Schaetzl, 2017).

65 In this context, we investigate the role of wind in triggering shallow landslides in the temperate  
66 rainforests of Chilean Patagonia. This mountainous region is exposed to high westerly winds that  
67 bring large amounts of rain from the Pacific, but has been featured rarely in landslide studies  
68 (Korup et al., 2019; Sepúlveda et al., 2010; Somos-Valenzuela et al., 2020). Our objective is to  
69 explore the combined effects of forest cover and wind speed, grouped by different topographic  
70 positions, on predicting landslides in rainforests in three study areas of south-central Chile  
71 (**Figure 1**).

72

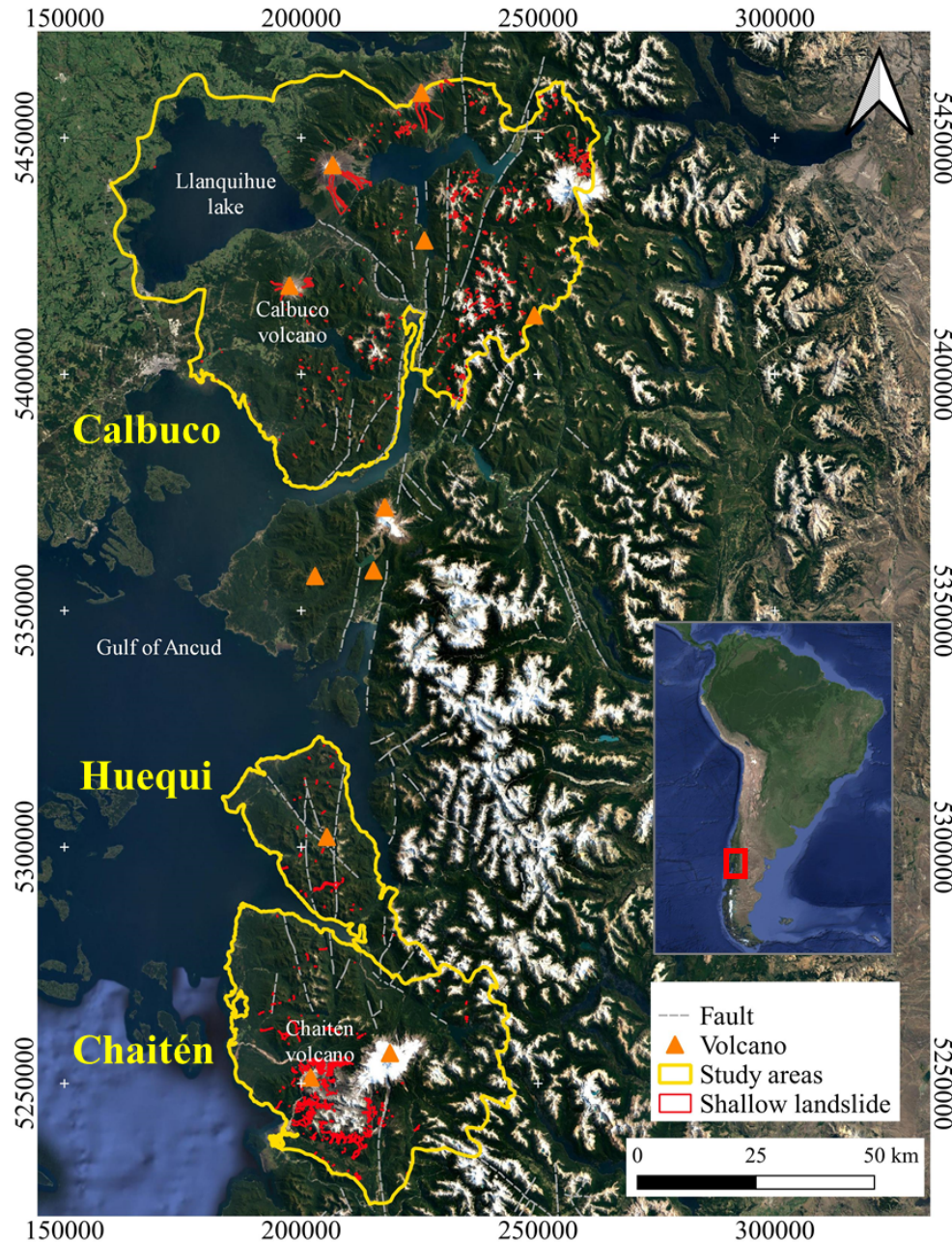
## 73 **2. Study areas**

74 The regional tectonic setting is characterized by active oblique subduction of the Nazca oceanic  
75 plate along the Southern Chile Trench and intra-arc dextral transpressional motion along the  
76 Liquiñe-Ofqui Fault zone in the southern Andes; Quaternary arc volcanism is active in the  
77 Southern Volcanic Zone (**Figure 1**). The western fringe of the Andes features steep mountainous  
78 terrain that was extensively glaciated (Singer, et al., 2004), and numerous cirques and small  
79 glaciers occupy headwaters today. The predominant soils are 1-2 m deep Andosols (Mohr et al.,

80 2017) on top of Pleistocene volcanic sediments covering a basement of Miocene granitoids and  
81 Paleozoic schists and gneisses (Piña-Gauthier et al., 2013).

82 The regional climate is humid, with annual precipitation totals of 3000-3200 mm (Alvarez-  
83 Garreton et al., 2018; Mohr et al., 2017) and a mean annual temperature of 8 °C (Alvarez-  
84 Garreton et al., 2018).

85 Our study areas are largely covered by stands of Valdivian temperate rainforests, which are  
86 structurally complex with many endemic species (DellaSala, 2011). The living biomass is high  
87 (~370 tC/ha) and up to twice as much organic carbon may reside in floodplain forest soils around  
88 Chaitén (**Figure 1**; (Mohr et al., 2017). Broadleaf species dominate these rainforest, while  
89 conifers are rare. Prominent tree species include *Nothofagus nitida* (Phil.) Krasser (coigue de  
90 Chiloé); *Podocarpus nubigenus* Lindl. (Manio); *Drimys winterii* J.R.Forst and G.Forst (canelo);  
91 *Amomyrtus meli* (Phil.) D.Legrand and Krausel (meli); and *Luma apiculata* (DC.) Burret  
92 (Arrayán rojo). Rainforest stands around Chaitén are in various states of post-volcanic  
93 disturbance initiated by the 2008 eruption sequence of Chaitén Volcano (Lara, 2009). The  
94 eruption gave rise to pyroclastic density currents, small lateral blasts, lava-dome growth and  
95 collapse, lahars and widespread tephra (Alfano et al., 2011). Subsequent reworking of  
96 volcanoclastic sediments aggraded river channels and floodplain forests by up to 11 m, causing  
97 channel avulsions, bank erosion, and log jams (Major et al., 2016; Pierson et al., 2013; Swanson  
98 et al., 2013). Tephra damaged on hillslope forests triggered a pulsed and distinctly delayed  
99 increase in landslide activity several years after the eruption (Korup et al., 2019).



101  
 102 **Figure 1.** Distribution of landslides mapped from 2001 to 2019 in the three study areas (yellow  
 103 borders) in south-central Chile: Calbuco (5880 km<sup>2</sup>), Huequi (897 km<sup>2</sup>) and Chaitén (2413 km<sup>2</sup>).  
 104 Faults are part of the greater active Liquiñe-Ofqui Fault Zone. Hydrographic data are from the  
 105 Dirección General de Aguas de Chile (DGA); geological data are from the National Geology and  
 106 Mining Service of Chile (SERNAGEOMIN). Coordinate system is UTM 19S; satellite imagery  
 107 is from Google Earth®.

108 **3 Methods**

109 3.1 Data

110 We compiled inventories of landslides that occurred in our study areas between 2001 and 2019  
111 by mapping from Google Earth® imagery and carrying out several local ground checks between  
112 2014 and 2019. We mapped landslides using diagnostic features such as distinct, elongate, and  
113 contrast-rich forest gaps with bare scarps showing displaced soil, and rock together with  
114 transport zones and runout lobes (Fiorucci et al., 2011). We mapped polygons approximating the  
115 total affected area for each landslide, estimating the date of each landslide with approximately  
116 annual precision that we obtained from the difference in timestamps of the images showing the  
117 latest undisturbed conditions and the earliest landslide occurrence. The triggers of these  
118 landslides remain unknown, though we can largely exclude seismic effects: the *M*7.6 Chiloé  
119 earthquake in 2016 (43.406°S, 73.941°W) was the largest recent near our study areas, though  
120 triggered 5% of the landslides in our study areas at the most. We mapped a total of 411  
121 landslides in Calbuco, 38 in Huequi, and 616 in Chaitén, covering 0.6%, 0.4% and 0.8% of each  
122 study area.

123 We used forest-cover information from the Global Forest Change inventory (Version 1.7)  
124 (Hansen, 2013) as a proxy of tree canopy cover in 2000, thus giving an indication about forest  
125 stands prior to all landslides that we mapped. Tree cover is defined as the fraction of canopy  
126 closure for >5 m high vegetation classified from time series of Landsat images at 30-m  
127 resolution ([https://earthenginepartners.appspot.com/science-2013-global-](https://earthenginepartners.appspot.com/science-2013-global-forest/download_v1.7.html)  
128 [forest/download\\_v1.7.html](https://earthenginepartners.appspot.com/science-2013-global-forest/download_v1.7.html)). Given the mostly high (>80%) crown closure in most of our study

129 area, we used a  $\log_{1p}$ -transformation of tree cover to reduce the strong negative skew in its  
130 distribution; we thus obtain a complementary metric of crown openness.

131 Regional data on wind speed have become widely available given the rising interest in the  
132 potential for clean and renewable power generation. We used wind speed (m/s) estimates from  
133 the Worldclim dataset (Fick & Hijmans, 2017), available as monthly averages for the period  
134 1970-2000. These data were generated based on weather station data interpolated with elevation,  
135 distance from the coast, and mean MODIS cloud cover as covariates at 1-km grid resolution. We  
136 aggregated these data to mean annual wind speeds (Figure S1, Supporting Information).

137 To characterize topographic position, we used SAGA GIS 2.3.2 and its landform classification  
138 tool by Weiss (2001) to derive a multi-scale Topographic Position Index (TPI) from 30-m  
139 elevation data from the Shuttle Radar Topography Mission (SRTM). The TPI compares the  
140 elevation of each pixel in a digital elevation model (DEM) to the mean elevation of a circular  
141 neighborhood around the pixel. To find a compromise between local landform detail and the  
142 wind-data resolution, we classified landform types by averaging over two neighborhoods of 100  
143 m and 1000 m.

### 144 3.2 Bayesian multilevel model

145 To analyze the role of crown openness and wind speed on the occurrence of shallow landslides  
146 we used logistic regression. This method has been used widely for landslide susceptibility studies  
147 due to its simplicity and ease of interpreting parameters (Das et al., 2012). We chose a Bayesian  
148 variant of logistic regression that admits prior knowledge about the parameters and explicitly  
149 handles uncertainties and sparse, imbalanced data (Bürkner, 2017; van de Schoot et al., 2021).

150 We chose a hierarchical model (Kruschke & Vanpaemel, 2015) because we surmise that

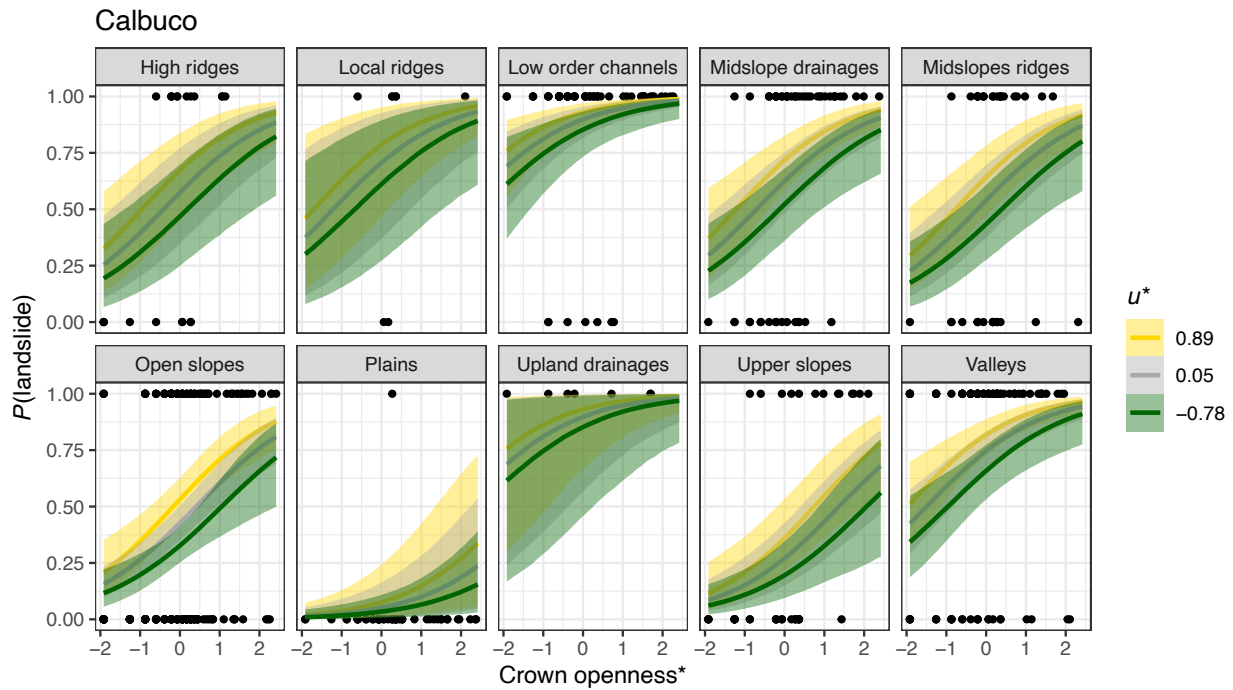
151 landslide occurrence, crown openness, and wind speed vary with landform type, hence  
152 acknowledging structure in our data. The model predicts the probability of classifying a given  
153 location (pixel) as part of a mapped landslide  $P(L)$  as a function of crown openness and wind  
154 speed for each landform type and the average of all data. The hierarchical structure of the model  
155 learns from the data one pooled (or population-level) parameter estimate for all the data, and  
156 individual parameters estimates that express deviations (or group-level effects) from this average  
157 for each landform type (see Supporting Information). We chose a varying intercept model, in  
158 which the weights of crown openness and wind speed remain unchanged across all landform  
159 types, though with differing average landslide probability. During the learning process,  
160 parameter estimates can inform each other across groups, thus reducing the potential for  
161 overconfident and unduly high or low coefficient values (Kruschke, 2014).

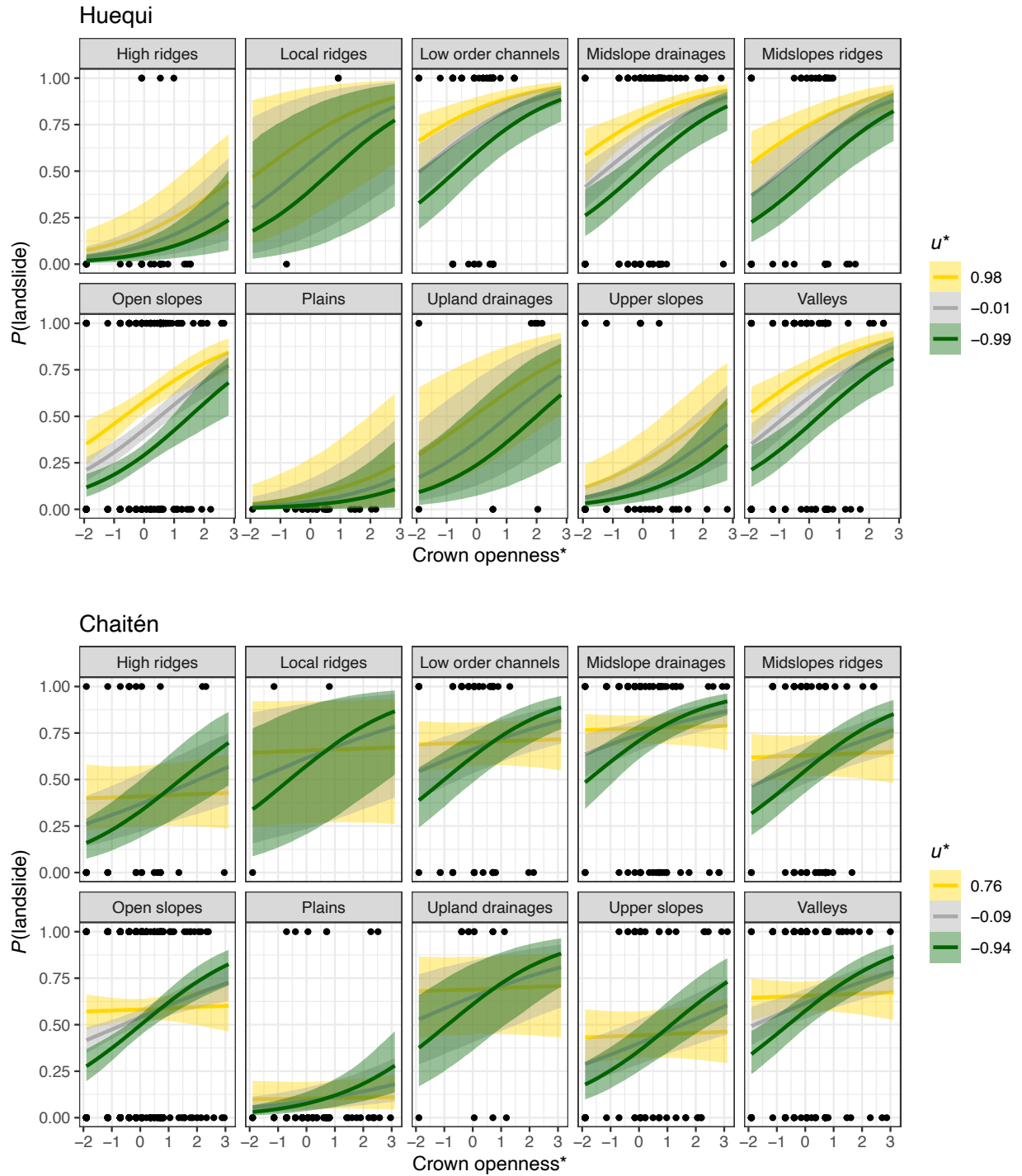
162 We use a weakly informative, but robust, Student- $t$  prior distribution for both crown openness  
163 and wind speed, and for the (population-level) intercept; for the standard deviation of group-level  
164 (landform) effects we chose a standard exponential prior, assuming that a lower variance of  $P(L)$   
165 between landforms is more likely than a higher one. We standardized all predictors to zero  
166 means and unit standard deviations and sampled from the numerically approximated posterior  
167 distribution given training data with a balanced number of landslide and unaffected terrain  
168 samples. We used the NUTS sampling scheme implemented in the STAN probabilistic  
169 programming language (Carpenter et al., 2017) to draw samples from the joint posterior  
170 distribution via the **R** package `brms` (Bürkner, 2017). We ran four independent Hamiltonian  
171 Monte Carlo chains based on 2000 iterations including 500 warm-up samples and checked each  
172 chain for convergence. We assessed the performance of this classifier based on its posterior

173 predictive distribution and recorded the fraction of correct classifications compared to the  
 174 observed frequency of landslides in all study areas and for all landform types.

175 **4 Results**

176 In all three study areas, the posterior distributions show that different landform types have  
 177 credibly different model intercepts and thus log-odds ratios of classifying landslides (Figure S2).  
 178 For an average crown openness and wind speed, the posterior probability of classifying a  
 179 location as part of a landslide is highest in midslope locations and low-order channels and their  
 180 adjacent hillslopes, and lowest on upper slopes and (mostly flood and coastal) plains (Figure 2).





182

183

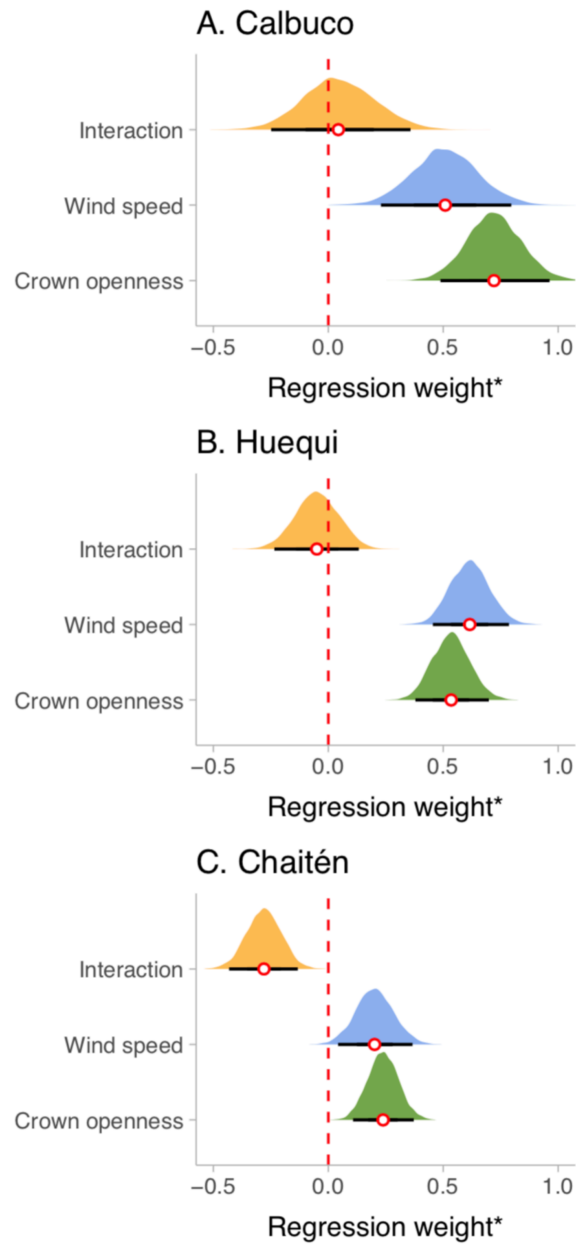
184 **Figure 2.** Posterior estimates of the probability of classifying a landslide based on standardized  
 185 predictors crown openness and wind speed  $u^*$  in our three study areas (Figure 1). Thick lines are  
 186 posterior medians, and shaded areas enclose the 95% highest density intervals for mean wind

187 speed (grey), and roughly one standard deviation above (gold) and below (green). Black dots are  
188 observed data.

189

190 Both crown openness and wind speed have positive credible and similar weights around Calbuco  
191 and Huequi, but roughly half their weight around Chaitén (**Figure 3**). The probability of  
192 classifying landslide terrain  $P(L)$  increases with crown openness and wind speed in all areas. For  
193 a fixed crown openness,  $P(L)$  changes with wind speed, except for the Chaitén area, which is the  
194 only area with a credible negative interaction between these two predictors. There,  $P(L)$  is nearly  
195 unchanged at high wind speeds regardless of forest cover (**Figure 2**). While the model predicts  
196 that  $P(L)$  increases with increasing wind speed in more dense forests around Chaitén, this  
197 relationship is reversed and lower wind speeds raise  $P(L)$  in more open forest stands.

198



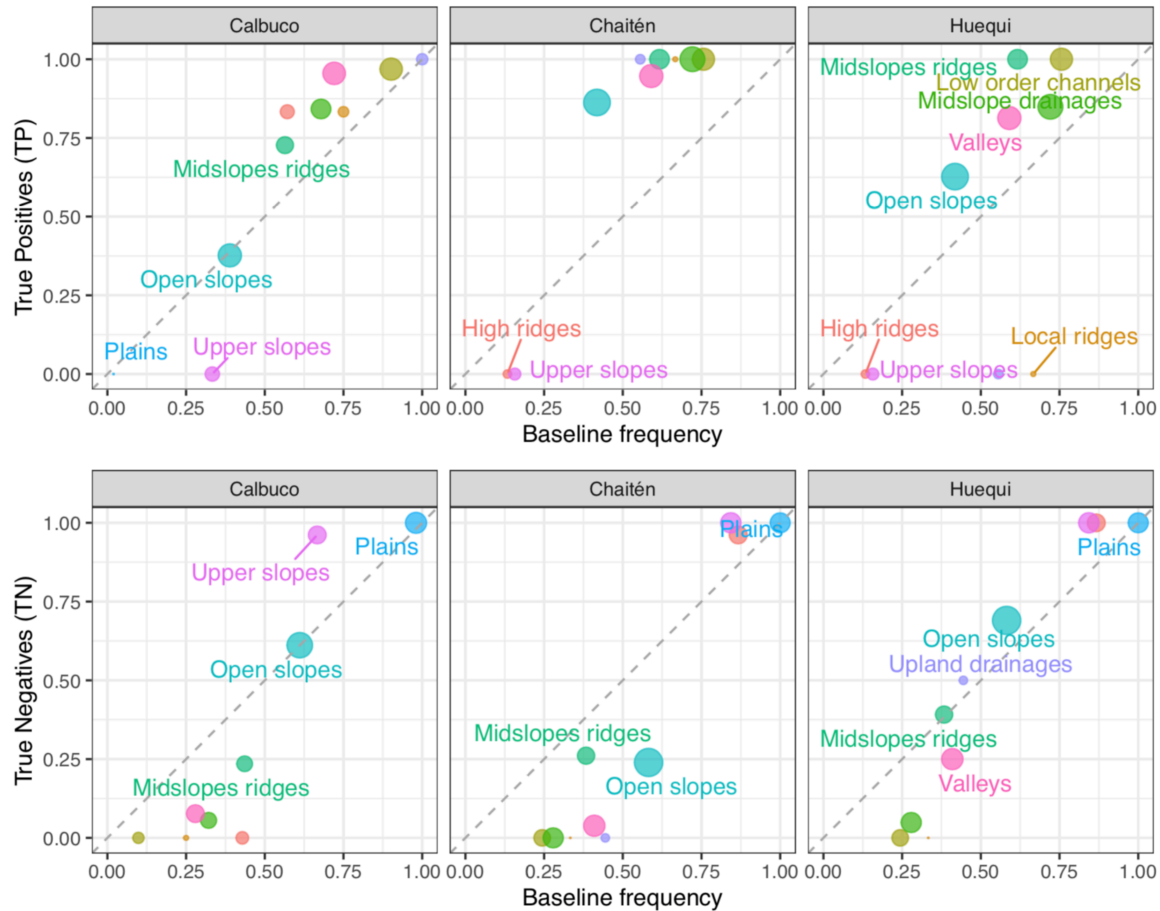
199

200 **Figure 3.** Posterior regression weights of standardised crown openness, wind speed, and their  
 201 interaction. Black horizontal lines are 95% highest density intervals, and white circles are  
 202 posterior means. Interaction between crown openness and wind speed is credibly non-zero only  
 203 in the Chaitén area.

204

205 The model performance at the level of each study area is moderate: the true positive rates are  
206 0.75 on average, and mostly higher than the average true negative rates, which are 0.52 on  
207 average (Figure S3). We note that models trained for Calbuco and Huequi have less average  
208 predictive skill for the volcanically disturbed Chaitén area, where 97% of mapped landslides and  
209 96% of the total landslide area occurred after the 2008 eruption sequence (Korup et al., 2019).  
210 However, the model trained for this particular area predicts landslides in the less or undisturbed  
211 study areas much better (though absence of landslides much worse). The average performance of  
212 all models improves substantially to true positive rates  $>0.8$  if considering individual landform  
213 types in the hierarchical model (**Error! No se encuentra el origen de la referencia.**). This  
214 improvement holds for most landforms except for high and local ridges and upper slopes, for  
215 which the model predicts true negative rates (landslide absence) better.

216



217

218 **Figure 4.** Model performance expressed as the true positive and true negative rates versus  
 219 empirically observed frequencies of landslide per landform type (colour-coded). Dashed grey  
 220 lines mark the baseline frequency of landslides (or their absence) and thus a purely random  
 221 classifier. Bubbles are scaled by observed landslides per landforms. Bubbles above (below) the  
 222 grey lines are posterior estimates that are better (worse) than the baseline.

223

## 224 **5 Discussion**

225 We explored the roles of forest cover and wind speed in predicting shallow landslides that  
 226 occurred in Chilean Patagonia between 2001 and 2019. Our statistical approach is based on the

227 assumption that the satellite-derived forest cover (Hansen, 2013) is sufficiently well resolved and  
228 accurate and representative of ecologically intact forest structure at the regional scale. Our  
229 balanced sample of landslide and unaffected terrain pixels is large enough to outweigh the role of  
230 possible outliers (such as local pixel noise or sensor artifacts) that we cater to by choosing a  
231 robust logistic regression. We acknowledge that the wind speed data are interpolated averages  
232 over at least three decades prior to the landslides that we mapped, and that more refined models  
233 could use synoptic data of wind fields and their variability as predictors. Averaged monthly wind  
234 speed may poorly reflect effects of gusts or windstorms. We therefore consider our estimates of  
235 the wind effects on landslides as conservative. Nonetheless, elevation is one foundation of these  
236 regionally interpolated wind speed estimates, and we expect that the data are consistent in this  
237 regard, collapsing effects of elevation and distance from the ocean (Fick & Hijmans, 2017).  
238 Measurements of wind directions in our study area highlight the role of wind exposure (Letelier  
239 et al., 2011) (Figure S4). An alternative model, however, in which the coefficients of crown  
240 openness and wind speed were allowed to vary across landforms revealed that neither predictor  
241 had weights that deviated credibly from the pooled average.

242 Another source of uncertainty and potential source of model misclassification is linked to the  
243 landslide inventory. Our mapping may underestimate the occurrence of smaller failures under  
244 forest cover mostly due to image resolution and shadow effects (Brardinoni et al., 2003). Yet we  
245 mapped landslides that happened since 2001, thus avoiding older imager with lower resolution.  
246 Several images taken after the eruption of the Chaitén volcano (2008) have artifact noise in  
247 tephra-covered areas and may under-represent landslide numbers. Some of the mapped  
248 landslides may have had failure surfaces too deep-seated to be affected by high wind loads, and  
249 we may have misclassified these deep-seated failures as shallow landslides. During our field

250 surveys, we observed that root networks often spread laterally above the soil-bedrock interface,  
251 with only few smaller roots penetrating several to tens of centimeters into bedrock cracks. Hence  
252 some of the landslides that we mapped and that our model misclassified may have involved more  
253 fractions of rock debris than mechanical stresses transferred by tree roots alone could mobilize.

254

255 Keeping these caveats in mind, our results support the notion that denser tree cover reduces the  
256 probability of classifying landslide terrain in a Bayesian framework. We find that wind speed has  
257 a comparable weight (Figure 3) with higher wind speeds predicting higher probabilities of  
258 classifying landslides. We also observe that the Chaitén area shows the largest differences in the  
259 weights and interaction of these predictors. There, the probability of classifying landslides in  
260 areas of high wind speed hardly changes with forest cover (Figure 2). We attribute this  
261 conspicuous difference to the 2008 eruptions of Chaitén volcano, which buried  $>150 \text{ km}^2$  of  
262 temperate rainforest under tephra (Korup et al., 2019), causing die-back of tree cohorts due to  
263 toxic fallout, stomata plugging, and local loads, causing hundreds of shallow landslides that  
264 dominate our inventory in this study area. The defoliation of disturbed tree cohorts may have  
265 reduced the surface area exposed to wind loads and thus lowered the effects of high winds  
266 (Swanson et al., 2013). In contrast, less windy areas with low or disturbed tree cover are more  
267 likely to feature landslides under our model. Such low-wind speed areas may have favored  
268 deposition of tephra and hence accumulated thicker layers that promote the decay of dead roots,  
269 thus decreasing root cohesion (Sidle, 1991) particularly on wind-protected sites. We emphasize  
270 that the Calbuco area was also impacted by a volcanic eruption in 2015, but to a much lesser  
271 extent with smaller areas of forest dieback and fewer post-eruptive landslides. We attribute only  
272 19% of the mapped landslides (or 10% of the total area) to the Calbuco eruption.

273

274 Overall, our findings about the role of wind speed are in line with those by Buma & Johnson  
275 (2015), who identified wind exposure as an important control for landslide initiation in the  
276 temperate rainforests of southeast Alaska. There, wind sheltered areas were devoid of evidence  
277 of major storms in the past 1000 years (Nowacki & Kramer, 1998), whereas wind-exposed  
278 slopes were disturbed by shallow landslides frequently (Kramer et al., 2001). Our model shows  
279 that wind speed without any information on direction can be an important predictor. While we  
280 would prefer wind speed squared  $u^2$  as the physically more meaningful predictor, our data are  
281 monthly means, so that squaring them would yield underestimates, as  $(E(u))^2 < E(u^2)$ , where  $E$  is  
282 the expectation value.

283

284 In essence, our results demonstrate the advantage of using a hierarchical model admitting  
285 landform types over several ones that simply average over all landforms in a given study area  
286 (**Figure 4**). The predictive performance increases notably for some landforms, though at the cost  
287 of underpredicting landslides on other landforms. Upper hillslopes and high ridges seem the most  
288 problematic areas for our model in terms of negligible skill, whereas it can predict landslides in  
289 low-order channels, midslope ridges or valleys confidently in regions outside of the training  
290 areas. One reason for the less skilled predictions may be that our model ignores the structure or  
291 edge effects of forest patches (Ruck et al., 2012) that can locally modify wind patterns and speed  
292 (Pawlik, 2013). Such edge effects may emphasize the gradual expansion of landslide-affected  
293 areas by either the retrogressive erosion of scarps or the downslope migration of deposit lobes by  
294 reworking. While our random sampling scheme to obtain training data minimizes spatial

295 autocorrelation in the predictors, the spatial association of topography, forest structure, and wind  
296 speed distribution may indeed drive more slope instability than our model detects.

297

298 Our model intentionally excludes the role of rainfall as one of the most plausible triggers of  
299 landslides in southern Chile. The high annual rainfall totals that can exceed 3,000 mm in our study  
300 areas make precipitation rarely a limiting factor on landslides (Buma & Johnson, 2015). We  
301 suspect that wind speed correlates with precipitation metrics (Rulli et al., 2007), and that wind  
302 speed thus reflects to some degree also hydrological drivers of slope instability beyond the  
303 mechanical control of wind load. The high landslide counts that we observed in mostly low-order  
304 channels and their neighbouring hillslopes (79% of all landslides in Calbuco, 63% in Huequi,  
305 and 43% in Chaitén) also point to hydrological triggers. While these topographic depressions  
306 collect more water, they also favor denser tree cover and funnel winds, however. We stress that  
307 our model prediction is also independent of local slope inclination, which is the dominant  
308 predictor of slope instability in comparable landslide susceptibility models (Reichenbach et al.,  
309 2018). Local elevation differences define the topographic position index, on which our landform  
310 classification is based. Yet these landforms are groups instead of predictors in our model.  
311 Moreover, the linear correlation between wind speed and local slope inclination ( $0.28 < r < 0.40$ )  
312 in our study areas is too low to attribute the role of wind speed to effects of hillslope steepness  
313 alone.

314

315 In summary, we see two immediate benefits from our hierarchical modeling approach. First, it  
316 helps to improve model performance by structuring the data into topographic positions that are  
317 intuitive and objectively different from each other, whereas the popular alternative of using

318 instead more predictors is more prone to the risk of overfitting and collinearity. Second, grouping  
319 the model by landforms opens the way for more customized and optimized landslide prediction  
320 catered to specific topographic locations even if the bulk average prediction for a study area is  
321 low. The hierarchical structure also helps to identify more objectively those portions of the  
322 landscape, for which we need better data constraints for landslide prediction.

323

## 324 **6 Conclusions**

325 Our Bayesian hierarchical logistic regression shows that more crown openness of forests and  
326 higher wind speeds credibly raise the chance to detect landslide terrain in three mountainous  
327 areas sustaining temperate rainforest areas in southern Chile. Volcanic disturbance appears to  
328 smooth out the role of high wind speeds by making denser forest stands more prone to  
329 landslides, and more open stands less prone. Trees cohorts buried or suffocated by tephra are  
330 areas where altered rates of soil water infiltration and root decay may be more dominant drivers  
331 of slope instability than wind loads alone. In any case, distinguishing between landforms in a  
332 hierarchical model context substantially improves an otherwise moderate average performance of  
333 the classification, but also highlights topographic locations for which the prediction needs to be  
334 refined. Our model also encourages further enquiry into the rarely investigated role of wind  
335 speed in promoting slope instability in southern Chile and dense forested mountain regions  
336 elsewhere, especially with weather and wind extremes being on a projected rise in a warming  
337 world (Jung & Schindler, 2019; Rosende et al., 2019).

338 **Acknowledgments, Samples, and Data**

339 E.P. acknowledges funding by the Agencia Nacional de Investigación y Desarrollo, Chile  
340 (ANID) and the German Academic Exchange Service, Germany (DAAD). E.P. and O.K. and  
341 collected and analysed the data; all authors contributed equally to writing the manuscript.

342 We are going to upload a **R** notebook containing the full code and data for the Bayesian logistic  
343 regression to a public repository, pending the final decision on this manuscript.

344 The SRTM DEM data are available at: <https://www.earthexplorer.usgs.gov>

345 The wind speed data are available at: <https://www.worldclim.org/data/worldclim21.html>

346 The forest-cover data are available at: [https://earthenginepartners.appspot.com/science-2013-](https://earthenginepartners.appspot.com/science-2013-global-forest)  
347 [global-forest](https://earthenginepartners.appspot.com/science-2013-global-forest)

348

349 **References**

350 Alfano, F., Bonadonna, C., Volentik, A. C. M., Connor, C. B., Watt, S. F. L., Pyle, D. M., &

351 Connor, L. J. (2011). Tephra stratigraphy and eruptive volume of the May, 2008, Chaitén

352 eruption, Chile. *Bulletin of Volcanology*, 73(5), 613–630. <https://doi.org/10.1007/s00445->

353 010-0428-x

354 Alvarez-Garreton, C., Mendoza, P. A., Pablo Boisier, J., Addor, N., Galleguillos, M., Zambrano-

355 Bigiarini, M., Ayala, A., et al. (2018). The CAMELS-CL dataset: Catchment attributes and

356 meteorology for large sample studies-Chile dataset. *Hydrology and Earth System Sciences*,

357 22(11), 5817–5846. <https://doi.org/10.5194/hess-22-5817-2018>

358 Baumann, M., Ozdogan, M., Wolter, P. T., Krylov, A., Vladimirova, N., & Radeloff, V. C.

- 359 (2014). Landsat remote sensing of forest windfall disturbance. *Remote Sensing of*  
360 *Environment*, 143, 171–179. <https://doi.org/10.1016/j.rse.2013.12.020>
- 361 Brardinoni, F., Slaymaker, O., & Hassan, M. A. (2003). Landslide inventory in a rugged forested  
362 watershed: A comparison between air-photo and field survey data. *Geomorphology*, 54(3–  
363 4), 179–196. [https://doi.org/10.1016/S0169-555X\(02\)00355-0](https://doi.org/10.1016/S0169-555X(02)00355-0)
- 364 Buma, B., Batllori, E., Bisbing, S., Holz, A., Saunders, S. C., Bidlack, A. L., Zaret, K., et al.  
365 (2019). Emergent freeze and fire disturbance dynamics in temperate rainforests. *Austral*  
366 *Ecology*, 44(5), 812–826. <https://doi.org/10.1111/aec.12751>
- 367 Buma, B., & Johnson, A. C. (2015). The role of windstorm exposure and yellow cedar decline on  
368 landslide susceptibility in southeast Alaskan temperate rainforests. *Geomorphology*, 228,  
369 504–511. <https://doi.org/10.1016/j.geomorph.2014.10.014>
- 370 Bürkner, P. C. (2017). brms: An R package for Bayesian multilevel models using Stan. *Journal*  
371 *of Statistical Software*, 80(1). <https://doi.org/10.18637/jss.v080.i01>
- 372 Carpenter, B., Gelman, A., Hoffman, M. D., Lee, D., Goodrich, B., Betancourt, M., Riddell, A.,  
373 et al. (2017). Stan: A probabilistic programming language. *Journal of Statistical Software*,  
374 76(1). <https://doi.org/10.18637/jss.v076.i01>
- 375 Das, I., Stein, A., Kerle, N., & Dadhwal, V. K. (2012). Landslide susceptibility mapping along  
376 road corridors in the Indian Himalayas using Bayesian logistic regression models.  
377 *Geomorphology*, 179(December), 116–125.  
378 <https://doi.org/10.1016/j.geomorph.2012.08.004>
- 379 DellaSala, D. A. (2011). Temperate and Boreal Rainforests of the World: Ecology and  
380 Conservation. *Temperate and Boreal Rainforests of the World: Ecology and Conservation*,  
381 (January). <https://doi.org/10.5822/978-1-61091-008-8>

- 382 Fick, S. E., & Hijmans, R. J. (2017). WorldClim 2: new 1-km spatial resolution climate surfaces  
383 for global land areas. *International Journal of Climatology*, 37(12), 4302–4315.  
384 <https://doi.org/10.1002/joc.5086>
- 385 Fiorucci, F., Cardinali, M., Carlà, R., Rossi, M., Mondini, A. C., Santurri, L., Guzzetti, F., et al.  
386 (2011). Seasonal landslide mapping and estimation of landslide mobilization rates using  
387 aerial and satellite images. *Geomorphology*, 129(1–2), 59–70.  
388 <https://doi.org/10.1016/j.geomorph.2011.01.013>
- 389 García-Ruiz, J. M., Beguería, S., Alatorre, L. C., & Puigdefábregas, J. (2010). Land cover  
390 changes and shallow landsliding in the flysch sector of the Spanish Pyrenees.  
391 *Geomorphology*, 124(3–4), 250–259. <https://doi.org/10.1016/j.geomorph.2010.03.036>
- 392 Glade, T. (2003). Landslide occurrence as a response to land use change: A review of evidence  
393 from New Zealand. *Catena*, 51(3–4), 297–314. [https://doi.org/10.1016/S0341-](https://doi.org/10.1016/S0341-8162(02)00170-4)  
394 [8162\(02\)00170-4](https://doi.org/10.1016/S0341-8162(02)00170-4)
- 395 Hale, S. A., Gardiner, B., Peace, A., Nicoll, B., Taylor, P., & Pizzirani, S. (2015). Comparison  
396 and validation of three versions of a forest wind risk model. *Environmental Modelling and*  
397 *Software*, 68, 27–41. <https://doi.org/10.1016/j.envsoft.2015.01.016>
- 398 Hansen, M. C. (2013). *High-Resolution Global Maps of 21st-Century Forest Cover Change*.  
399 850(November), 850–854. <https://doi.org/10.1126/science.1244693>
- 400 Hilton, R. G., Galy, A., & Hovius, N. (2008). Riverine particulate organic carbon from an active  
401 mountain belt: Importance of landslides. *Global Biogeochemical Cycles*, 22(1), n/a-n/a.  
402 <https://doi.org/10.1029/2006GB002905>
- 403 Hilton, R. G., Meunier, P., Hovius, N., Bellingham, P. J., & Galy, A. (2011). Landslide impact  
404 on organic carbon cycling in a temperate montane forest. *Earth Surface Processes and*

- 405 *Landforms*, 36(12), 1670–1679. <https://doi.org/10.1002/esp.2191>
- 406 Johnstone, J. F., Allen, C. D., Franklin, J. F., Frelich, L. E., Harvey, B. J., Higuera, P. E.,  
407 Turner, M. G., et al. (2016). Changing disturbance regimes, ecological memory, and forest  
408 resilience. *Frontiers in Ecology and the Environment*, 14(7), 369–378.  
409 <https://doi.org/10.1002/fee.1311>
- 410 Jung, C., & Schindler, D. (2019). Changing wind speed distributions under future global climate.  
411 *Energy Conversion and Management*, 198(May).  
412 <https://doi.org/10.1016/j.enconman.2019.111841>
- 413 Korup, O., Seidemann, J., & Mohr, C. H. (2019). Increased landslide activity on forested  
414 hillslopes following two recent volcanic eruptions in Chile. *Nature Geoscience*, 12(4), 284–  
415 289. <https://doi.org/10.1038/s41561-019-0315-9>
- 416 Kramer, M. G., Hansen, A. J., Taper, M. L., & Kissinger, E. J. (2001). Abiotic controls on long-  
417 term windthrow disturbance and temperate rain forest dynamics in southeast Alaska.  
418 *Ecology*, 82(10), 2749–2768. [https://doi.org/10.1890/0012-9658\(2001\)082\[2749:ACOLTW\]2.0.CO;2](https://doi.org/10.1890/0012-9658(2001)082[2749:ACOLTW]2.0.CO;2)
- 420 Kruschke, J K, & Vanpaemel, W. (2015). Bayesian estimation in hierarchical models. *The*  
421 *Oxford Handbook of Computational and Mathematical Psychology*, (January), 279–299.  
422 <https://doi.org/10.1093/oxfordhb/9780199957996.013.13>
- 423 Kruschke, John K. (2014). Doing Bayesian data analysis: A tutorial with R, JAGS, and Stan,  
424 second edition. In *Doing Bayesian Data Analysis: A Tutorial with R, JAGS, and Stan*,  
425 *Second Edition*. <https://doi.org/10.1016/B978-0-12-405888-0.09999-2>
- 426 Lara, L. E. (2009). The 2008 eruption of the Chaitén Volcano, Chile: a preliminary report.  
427 *Andean Geology*, 36. <https://doi.org/10.4067/S0718-71062009000100009>

- 428 Lehmann, P., von Ruetten, J., & Or, D. (2019). Deforestation Effects on Rainfall-Induced Shallow  
429 Landslides: Remote Sensing and Physically-Based Modelling. *Water Resources Research*,  
430 55(11), 9962–9976. <https://doi.org/10.1029/2019WR025233>
- 431 Letelier, J., Soto-Mardones, L., Salinas, S., Osuna, P., López, D., Sepúlveda, H. H., Rodrigo, C.,  
432 et al. (2011). Variabilidad del viento, oleaje y corrientes en la región norte de los fiordos  
433 Patagónicos de Chile. *Revista de Biología Marina y Oceanografía*, 46(3), 363–377.  
434 <https://doi.org/10.4067/S0718-19572011000300007>
- 435 Luysaert, S., Schulze, E. D., Börner, A., Knohl, A., Hessenmöller, D., Law, B. E., Grace, J., et  
436 al. (2008). Old-growth forests as global carbon sinks. *Nature*, 455(7210), 213–215.  
437 <https://doi.org/10.1038/nature07276>
- 438 Major, J. J., Bertin, D., Pierson, T. C., Amigo, Á., Iroumé, A., Ulloa, H., & Castro, J. (2016).  
439 Extraordinary sediment delivery and rapid geomorphic response following the 2008-2009  
440 eruption of Chaitén Volcano, Chile. *Water Resources Research*, 52(7), 5075–5094.  
441 <https://doi.org/10.1002/2015WR018250>
- 442 Major, J. J., & Lara, L. E. (2013). Overview of Chaitén Volcano, Chile, and its 2008-2009  
443 eruption. *Andean Geology*, 40(2), 196–215. <https://doi.org/10.5027/andgeoV40n2-a01>
- 444 Mirus, B. B., Smith, J. B., & Baum, R. L. (2017). Hydrologic Impacts of Landslide  
445 Disturbances: Implications for Remobilization and Hazard Persistence. *Water Resources*  
446 *Research*, 53(10), 8250–8265. <https://doi.org/10.1002/2017WR020842>
- 447 Mohr, C. H., Korup, O., Ulloa, H., & Iroumé, A. (2017). Pyroclastic Eruption Boosts Organic  
448 Carbon Fluxes Into Patagonian Fjords. *Global Biogeochemical Cycles*, 31(11), 1626–1638.  
449 <https://doi.org/10.1002/2017GB005647>
- 450 Nowacki, G. J., & Kramer, M. G. (1998). The effects of wind disturbance on temperate rain

- 451 forest structure and dynamics of southeast Alaska. *USDA Forest Service - General*  
452 *Technical Report PNW*, (PNW-GTR-421).
- 453 O' Loughlin, C., & Ziemer, R. R. (1982). The Importance of Root Strength and Deterioration  
454 Rates Upon Edaphic Stability in Steepland Forests. *Proceedings of an IUFRO Workshop*,  
455 (August 1982), 70–78. <https://doi.org/10.1111/j.1471-8286.2005.00877.x>
- 456 Pallister, J., Major, J., Hoblitt, R., Lowenstern, J., Eichelberger, J., Lara, L., Crisafulli, C., et al.  
457 (2010). Interdisciplinary Studies of Eruption at Chaitén Volcano , Chile Atmospheric  
458 Remote Sensing on the International Space Station. *Eos, Transactions American*  
459 *Geophysical Union*, 91(42), 381–382.
- 460 Pawlik, L. (2013). The role of trees in the geomorphic system of forested hillslopes — A review.  
461 *Earth-Science Reviews*, 126, 250–265. <https://doi.org/10.1016/j.earscirev.2013.08.007>
- 462 Pierson, T. C., Major, J. J., Amigo, Á., & Moreno, H. (2013). Acute sedimentation response to  
463 rainfall following the explosive phase of the 2008-2009 eruption of Chaitén volcano, Chile.  
464 *Bulletin of Volcanology*, 75(5), 1–17. <https://doi.org/10.1007/s00445-013-0723-4>
- 465 Piña-Gauthier, M., Lara, L. E., Bataille, K., Tassara, A., & Báez, J. C. (2013). Deformación co-  
466 eruptiva y crecimiento del domo durante la erupción 2008-2009 del volcán chaitén, andes  
467 del sur. *Andean Geology*, 40(2), 310–323. <https://doi.org/10.5027/andgeoV40n2-a08>
- 468 Reichenbach, P., Rossi, M., Malamud, B. D., Mihir, M., & Guzzetti, F. (2018). A review of  
469 statistically-based landslide susceptibility models. *Earth-Science Reviews*, 180(November  
470 2017), 60–91. <https://doi.org/10.1016/j.earscirev.2018.03.001>
- 471 Rickli, C., & Graf, F. (2009). Effects of forests on shallow landslides - Case studies in  
472 Switzerland. *Forest Snow and Landscape Research*, 82(1), 33–44.
- 473 Rosende, C., Sauma, E., & Harrison, G. P. (2019). Effect of Climate Change on wind speed and

- 474 its impact on optimal power system expansion planning: The case of Chile. *Energy*  
475 *Economics*, 80, 434–451. <https://doi.org/10.1016/j.eneco.2019.01.012>
- 476 Ruck, B., Frank, C., & Tischmacher, M. (2012). On the influence of windward edge structure  
477 and stand density on the flow characteristics at forest edges. *European Journal of Forest*  
478 *Research*, 131(1), 177–189. <https://doi.org/10.1007/s10342-010-0451-7>
- 479 Rulli, M. C., Meneguzzo, F., & Rosso, R. (2007). Wind control of storm-triggered shallow  
480 landslides. *Geophysical Research Letters*, 34(3), 1–5.  
481 <https://doi.org/10.1029/2006GL028613>
- 482 Schwab, J. W. (1983). *Mass wasting: October–November 1978 storm, Rennell Sound, Queen*  
483 *Charlotte Islands, British Columbia*.
- 484 Schwarz, M., Lehmann, P., & Or, D. (2010). Quantifying lateral root reinforcement in steep  
485 slopes - from a bundle of roots to tree stands. *Earth Surface Processes and Landforms*,  
486 35(3), 354–367. <https://doi.org/10.1002/esp.1927>
- 487 Sepúlveda, S. A., Serey, A., Lara, M., Pavez, A., & Rebolledo, S. (2010). Landslides induced by  
488 the April 2007 Aysén Fjord earthquake, Chilean Patagonia. *Landslides*, 7(4), 483–492.  
489 <https://doi.org/10.1007/s10346-010-0203-2>
- 490 Sidle, R. C. (1991). A Conceptual Model of Changes in Root Cohesion in Response to  
491 Vegetation Management. *Journal of Environmental Quality*, 20(1), 43–52.  
492 <https://doi.org/10.2134/jeq1991.00472425002000010009x>
- 493 Singer, B. S., Ackert, R. P., & Guillou, H. (2004).  $^{40}\text{Ar}/^{39}\text{Ar}$  and K-Ar chronology of  
494 Pleistocene glaciations in Patagonia. *Bulletin of the Geological Society of America*, 116(3–  
495 4), 434–450. <https://doi.org/10.1130/B25177.1>
- 496 Sommerfeld, A., Senf, C., Buma, B., D'Amato, A. W., Després, T., Díaz-Hormazábal, I., ...

- 497 Seidl, R. (2018). Patterns and drivers of recent disturbances across the temperate forest  
498 biome. *Nature Communications*, 9(1). <https://doi.org/10.1038/s41467-018-06788-9>
- 499 Somos-Valenzuela, M. A., Oyarzún-Ulloa, J. E., Fustos-Toribio, I. J., Garrido-Urzuza, N., &  
500 Chen, N. (2020). The mudflow disaster at Villa Santa Lucía in Chilean Patagonia:  
501 understandings and insights derived from numerical simulation and postevent field surveys.  
502 *Natural Hazards and Earth System Sciences*, 20(8), 2319–2333.  
503 <https://doi.org/10.5194/nhess-20-2319-2020>
- 504 Swanson, F. J., Jones, J. A., Crisafulli, C. M., & Lara, A. (2013). Effects of volcanic and  
505 hydrologic processes on forest vegetation: Chaitén Volcano, Chile. *Andean Geology*, 40(2),  
506 359–391. <https://doi.org/10.5027/andgeoV40n2-a10>
- 507 Valtera, M., & Schaetzl, R. J. (2017). Pit-mound microrelief in forest soils: Review of  
508 implications for water retention and hydrologic modelling. *Forest Ecology and*  
509 *Management*, 393, 40–51. <https://doi.org/10.1016/j.foreco.2017.02.048>
- 510 van de Schoot, R., Depaoli, S., King, R., Kramer, B., Märten, K., Tadesse, M. G., Yau, C., et al.  
511 (2021). Bayesian statistics and modelling. *Nature Reviews Methods Primers*, 1(1), 1.  
512 <https://doi.org/10.1038/s43586-020-00001-2>
- 513 Veblen, T. ., & Alaback, P. (1996). High-Latitude Rainforests and Associated Ecosystems of the  
514 West Coast of the Americas. *High-Latitude Rainforest and Associated Ecosystems of the*  
515 *West Coast of the Americas*, 116(March), 173–213. [https://doi.org/10.1007/978-1-4612-](https://doi.org/10.1007/978-1-4612-3970-3)  
516 [3970-3](https://doi.org/10.1007/978-1-4612-3970-3)
- 517 Weiss, A. D. (2001). *Topographic Positions and Landforms Analysis (conference poster)*. ESRI  
518 *International User Conference*. San Diego, CA. 200. Retrieved from  
519 [http://www.jennessent.com/downloads/TPI-poster-TNC\\_18x22.pdf](http://www.jennessent.com/downloads/TPI-poster-TNC_18x22.pdf)

# Supporting Information for ”Predicting Patagonian Landslides: Roles of Forest Cover and Wind Speed”

Eric Parra<sup>1,2</sup>, Christian Mohr<sup>1</sup>, Oliver Korup<sup>1,2</sup>

<sup>1</sup>Institute of Environmental Science and Geography, University of Potsdam, Germany

<sup>2</sup>Institute of Geosciences, University of Potsdam, Germany

## Contents of this file

1. Text S1
2. Figures S1 to S4

## Introduction

This file contains supporting text devoted to outline the model setup and additional figures that expand on the results documented in the main manuscript.

**Text S1.** We used a Bayesian robust regression to predict the posterior probability  $P(L)$  at which a given location  $y_i$  in our study areas is classified as part of a landslide source, transport, or deposition area. We write this as  $P(L) = P(y_i = 1)$  and denote the inverse probability of classifying a location without a landslide as  $P(y_i = 0) = 1 - P(y_i = 1)$ . The index  $i$  refers to the  $i$ th location, i.e. raster value, out of  $n$  observations in given study

---

area. We can write this model with a Bernoulli likelihood conditional on the observed data in general form as:

$$P(y_i = 1 | \mathbf{X}_i, \mathbf{w}) = \frac{1}{1 + e^{-\mathbf{X}_i \mathbf{w}}}, \quad (1)$$

where  $\mathbf{X}_i$  is the  $i$ th row in a  $n \times m$  design matrix with  $n$  observations and  $m$  columns. The first column consists of 1's for the intercept, while the remaining  $m - 1$  columns collect the predictor (and possible interaction) values. The  $m \times 1$  column vector  $\mathbf{w}$  contains the  $m$  model coefficients, i.e. the intercept, the predictor weights, and weights for interaction terms, if any. The matrix-vector product  $\mathbf{X}_i \mathbf{w}$  constitutes the linear predictor of the model.

We acknowledge structure in our data by admitting  $j = \{1, \dots, 10\}$  different grouping levels  $l_j$  to the model. These levels represent ten landform types that we classified from the Topographic Position Index. We standardised the input values to zero means and unit standard deviations and designate standardised parameters with an asterisk (\*). In this hierarchical (or multilevel) model structure, we use as inputs standardised crown openness  $\chi^*$  and standardised wind speed  $u^*$ , as well as their interaction  $\chi^*.u^*$  and write this for our specific case:

$$P(y_i = 1 | \mathbf{X}_i, \mathbf{w}) = \left( 1 + e^{-w_0[j] + w_1 \chi_i^* + w_2 u_i^* + w_3 \chi_i^*.u_i^*} \right)^{-1}, \quad (2)$$

where we allow the intercept  $w_0[j]$  to vary by landform type  $j$  as:

$$w_0[j] \sim \mathcal{N}(0, \sigma_j^2), \quad (3)$$

where  $\sigma_j^2$  is the variance of group-level intercepts, i.e. whether and by how much the log-odds ratios for average predictor inputs vary by landform type. Note that these intercepts represent log-odds ratios of classifying location  $y_i$  as part of a landslide for zero (i.e. average) predictor values. Positive log-odds ratios are equivalent to values of  $P(L) > 0.5$ , while negative log-odds ratios are equivalent to  $P(L) < 0.5$ . The zero mean of the Gaussian distribution in Equation 3 is the intercept of the model pooled over all data regardless of landform type.

We specify our prior assumptions using the following distributions:

$$w_0[j] \sim \mathcal{T}(\nu = 3, \mu = 0, \sigma = 2.5), \quad (4)$$

$$w_1 \sim \mathcal{T}(\nu = 3, \mu = 0, \sigma = 2.5), \quad (5)$$

$$w_2 \sim \mathcal{T}(\nu = 3, \mu = 0, \sigma = 2.5), \quad (6)$$

$$w_3 \sim \mathcal{T}(\nu = 3, \mu = 0, \sigma = 2.5), \quad (7)$$

These independent prior distributions are weakly informative and based on the assumption that all model weights are from a Student's  $t$ -distribution with location  $\mu = 0$  and scale  $\sigma = 2.5$ . This choice of prior means that we surmise that regression weights may be equally likely positive or negative, though symmetrically distributed and within the

interval  $[-7.96, 7.96]$  with 95% probability. Such extreme regression weights are unlikely for standardised predictors and underline our weakly informative choice.

Our prior distribution of the variance of the group-level intercept is a standard exponential. This reflects our assumption that the spread of log-odds of classifying landslides is more likely near zero, hence more likely to differ less with landform type:

$$\sigma_j \sim \exp(\lambda = 1), \quad (8)$$

This prior specifies that  $\sigma_j$  lies in the interval  $[0, 3]$  with 95% probability, with larger spread becoming exponentially less likely.

We ran our model with different parameter choices for these priors and observed only minute changes in the posterior distributions, given the large number of observations in each study area. Although using the three study areas as another grouping level in the model would be possible, we preferred using the data from the different regions as testing data for models trained elsewhere.

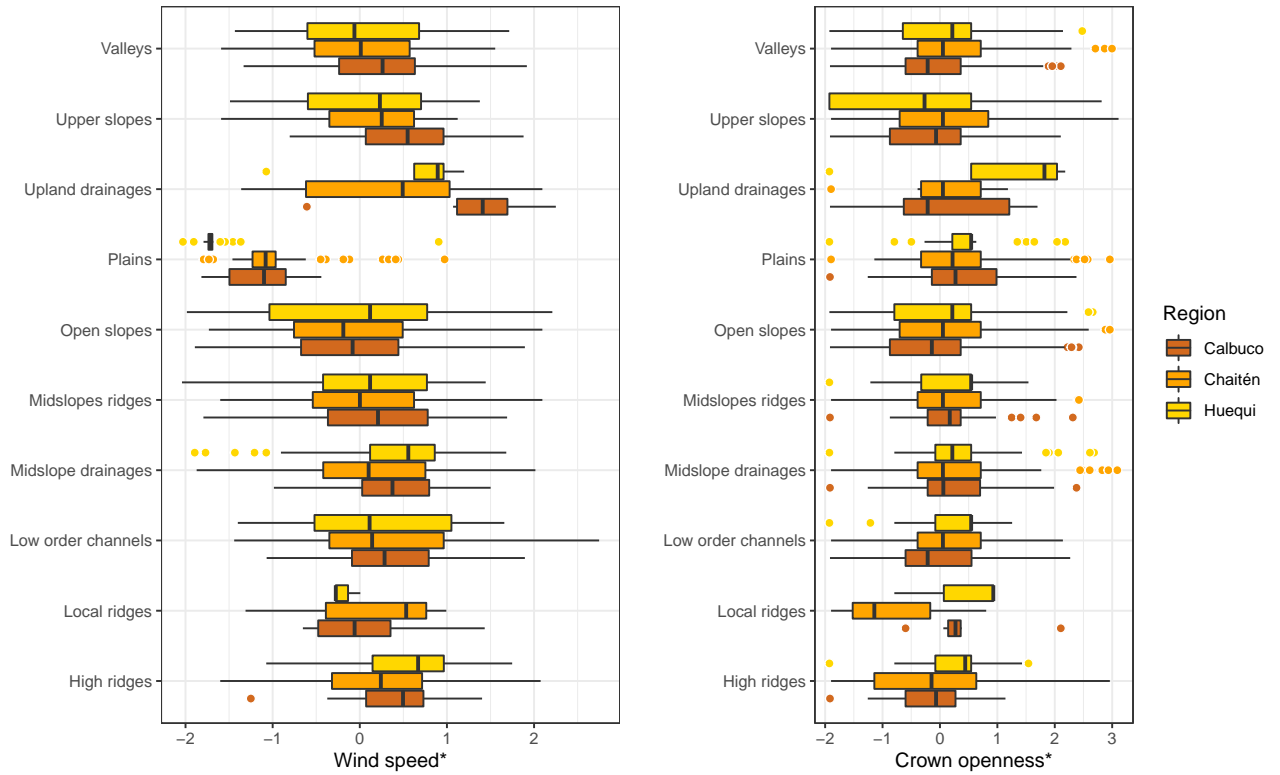


**Figure S1.** Distributions of standardised wind speed and standardised crown openness per landform type in temperate rainforests in three study areas of south-central Chile. Boxes encompass the interquartile range, and box centres are medians; whiskers span 1.5 times the interquartile range and points are outliers.

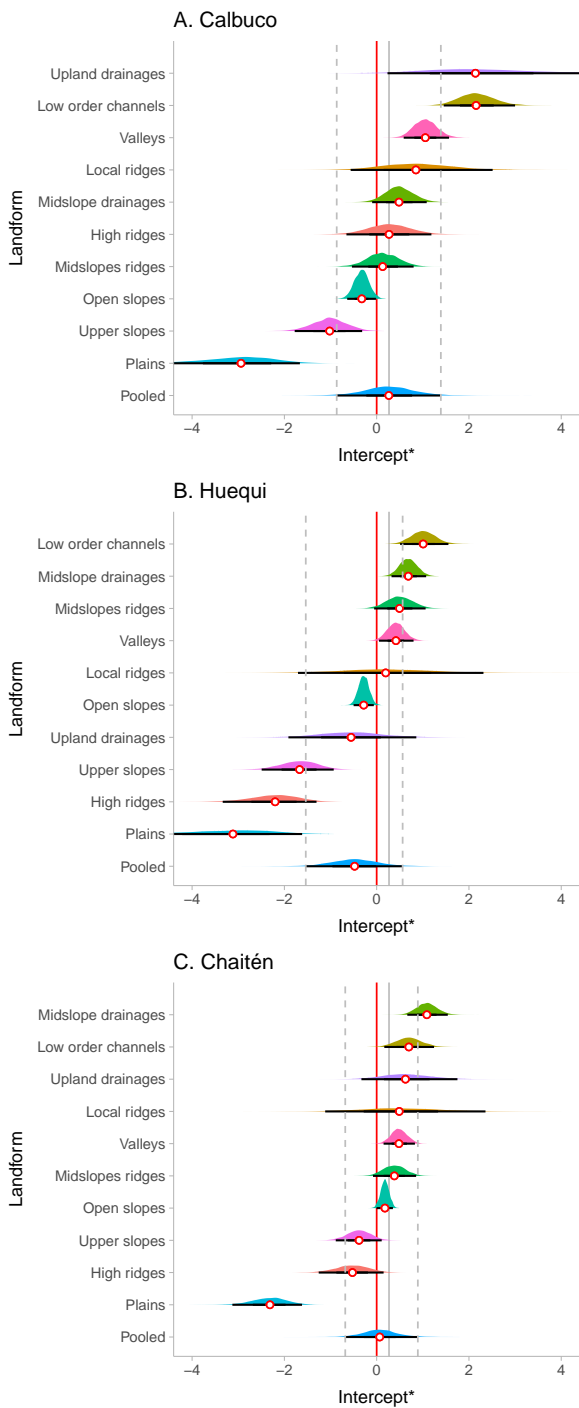


**Figure S2.** Posterior distributions of standardised model intercepts by landform type. Black horizontal lines are 95% highest density intervals (HDIs), and white circles are posterior means. Vertical grey solid (dashed) lines are pooled means (95% HDIs). Intercepts are the log-odds ratios of classifying a pixel with average crown openness and wind speed as part of a landslide.

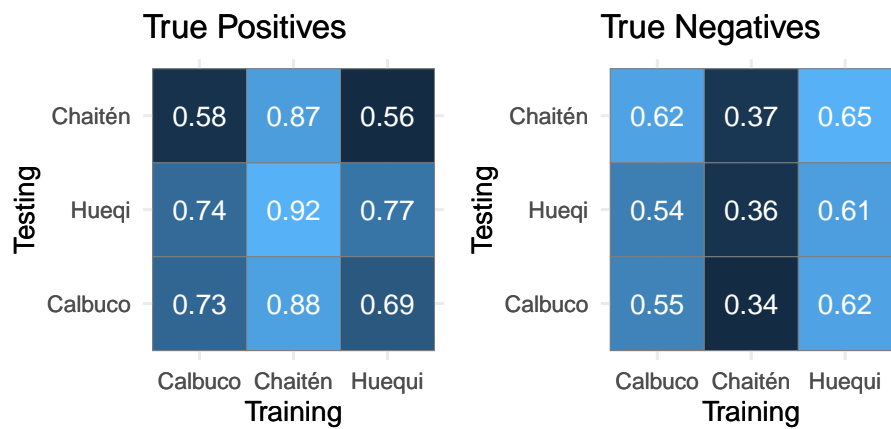


**Figure S3.** Performance of Bayesian robust logistic regression for predicting landslide terrain from crown openness and wind speed. True positive (and negative) rates refer to the fraction of correctly predicted landslides (and their absence) for a given training and testing dataset. All rates refer to the pooled model averaged over all landform types. The average true positive rate is 0.75, whereas the average true negative rate is 0.52.

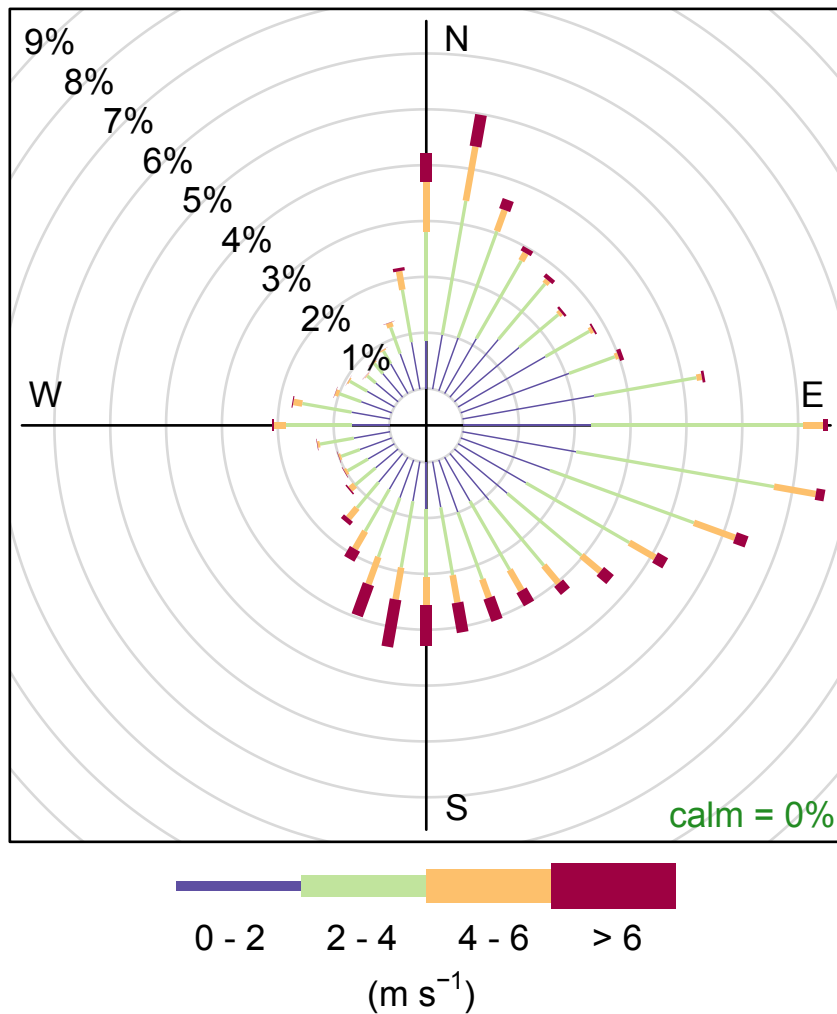


**Figure S4.** Rose diagram of hourly wind speed and direction for south-central Chile (40–43°S, 72–73°W) from January 2013 to December 2017; grey circles are the frequency of observations. The overall mean wind speed was  $2.9 \text{ m s}^{-1}$ , mostly from a W to WNW direction and with negligible amount of calm conditions. Data are freely available from the Global Forecast System (GFS) of the U.S. National Weather Service (NWS) at <https://www.ncdc.noaa.gov/data-access/model-data/model-datasets/globalforecast-system-gfs>.

March 25, 2021, 2:36pm